Materials Research. 2014; 17(5): 1344-1355
DOI: http://dx.doi.org/10.1590/1516-1439.306014

A Model for Evaluation of Effective Thermal Conductivity of Periodic Composites with Poorly Conducting Interfaces

Romildo S. Escarpini Filho*[a], *Severino Pereira Cavalcanti Marques*[b]

[a]*Federal University of Alagoas – UFAL, Campus do Sertão, Delmiro Gouveia, CEP 57480-000, Delmiro Gouveia, AL, Brazil*
[b]*Center of Technology, Federal University of Alagoas – UFAL, CEP 57072-900, Maceió, AL, Brazil*

Received: July 2, 2014; Revised: October 3, 2014

This paper presents a new micromechanical extension of the parametric finite-volume theory for evaluation of effective thermal conductivities of periodic unidirectional fiber reinforced composites. Such materials are assumed as composed of repeating unit cells with arbitrary internal architectural arrangements of fiber coated by thin interphase with low thermal conductivity. The parametric homogenization approach uses quadrilateral subvolumes for discretization of the repeating unit cell microstructure, thereby allowing an efficient modeling of the details of fibers with arbitrarily shaped cross sections. The interphases are replaced by imperfect interface elements with continuity in normal heat flux and discontinuity in temperature. The performance of the homogenization model is demonstrated for several numerical examples, including two-and three-phase composites with regular squared and hexagonal arrays of fibers. The ability of the model to accurately predict the effective thermal conductivity of those composites is demonstrated by means of comparisons of results obtained using finite-element and analytical solutions.

Keywords: *periodic composite materials, effective thermal conductivity, imperfect interfaces, homogenization, finite-volume theory*

1. Introduction

An important feature of the composite materials is their multifunctionality. They have encountered a very wide range of applications extending from heavy structural systems to micro or nanoelectronic devices. In many of these practical uses, the composite components cannot be safely designed without taking into account the relevant material thermal properties. The material thermal conductivities, for example, are indispensable quantities to describe the temperature fields used for the evaluation of the thermal stresses which have an important role in the mechanical behavior of many structural systems, particularly, for those subjected to severe non-isothermal environments. The effective thermal conductivities of composite materials depend on many factors, including properties and volume fractions of their constituents, as well as, microstructural characteristics, such as geometrical shapes, distributions of the reinforcement and interfaces between the matrix and inclusions.

A number of analytical and numerical micromechanical models have been formulated to calculate the effective thermal conductivity and stiffness of composite materials. Many of these analytical models have been developed for unidirectional two-phase fiber composites assuming a regular microstructure composed by repeating unit cells with particular geometrical shape and simple internal architectural arrangements[1-3]. For instance, to estimate analytically the effective stiffness of periodic composites, it can be mentioned the Periodic Microstructure Model (PMM)[4], which could be also explored to obtain effective thermal properties. However, for the cases of high volume fractions of fibers, as well as, high and low fiber-to-matrix thermal conductivity ratios, it is common that analytical micromechanical models for predicting the transverse thermal conductivities provide different results among themselves[5,6]. For more elaborated microstructure, however, the use of numerical procedures is needed for accurate predictions of the transverse effective thermal conductivity. In these latter modeling studies, the finite-element method is, typically, the more employed numerical technique.

An attractive alternative to the finite-element method in the solution of periodic repeating unit cell (RUC) problems is the parametric finite-volume theory developed by Cavalcante et al.[7] having as basis the original version constructed by Bansal and Pindera[8]. In that parametric version the heterogeneous material microstructure is discretized using quadrilateral subvolumes which are mapped into corresponding reference square subvolumes. This mapping has been incorporated into the standard finite-volume direct averaging micromechanics (FVDAM) model and applied successfully to solve several mechanical homogenization problems[9-11].

The purpose of this paper is to present a new micromechanical extension of the homogenized parametric finite-volume theory for evaluation of effective thermal conductivities of periodic unidirectional fiber reinforced

*e-mail: smarques@ctec.ufal.br

composites. Such materials are assumed as composed of replicated fundamental building blocks, called repeating unit cells, with arbitrary internal architectural arrangements of fiber coated by thin interphase with low thermal conductivity. The interphases are replaced by imperfect interface elements with continuity in normal heat flux and discontinuity in temperature. Indeed, the proposed computational procedure allows an easy and efficient treatment of the temperature discontinuity condition through the interfaces. The treatment of this temperature jump at an interface cannot be easily handled using the classical finite element method[12]. The performance of the homogenization model is demonstrated for several numerical examples, including composites with perfect and imperfect interfaces and different arrays of fibers. The numerical results are verified by means of comparisons with solutions obtained using analytical and finite element methods.

2. Preliminary Considerations on the Homogenization Problem

First, suppose a representative volume element (RVE) of a general composite material, with volume V and boundary surface S, subjected to a homogeneous temperature boundary condition given by

$$T^o(\boldsymbol{x}) = G_i^o x_i \text{ for } \boldsymbol{x} \in S \tag{1}$$

where $G_i^o = \partial T^o / \partial x_i$ (i = 1,2,3) are constants. The average temperature and the average temperature gradient vector taken over the RVE are defined respectively by

$$\langle T \rangle = \frac{1}{V}\int_V T(\boldsymbol{x})dV \tag{2}$$

$$\langle \boldsymbol{G} \rangle = \frac{1}{V}\int_V \boldsymbol{G}(\boldsymbol{x})dV \tag{3}$$

being $T(\boldsymbol{x})$ the temperature field and $\boldsymbol{G}(\boldsymbol{x})$ the corresponding temperature gradient vector whose components are given by $G_i(\boldsymbol{x}) = \partial T / \partial x_i$. Applying the divergence theorem to Equation 3, the following relation is obtained for the temperature gradient components

$$\langle G \rangle_i = \frac{1}{V}\int_S T^o(\boldsymbol{x}) n_i(\boldsymbol{x}) dS \tag{4}$$

with n_i denoting the i th component of the outward unit vector normal to the surface S. The substitution of Equation 1 into Equation 4 yields

$$\langle G \rangle_i = G_i^o \tag{5}$$

meaning that the components of the average temperature gradient over the entire RVE coincide with the corresponding components of the temperature gradient on the RVE boundary surface S, irrespective of the material microstructure. Equation 5 corresponds to the Average Temperature Gradient Theorem.

Now, consider that the composite material has a periodic microstructure, which can be generated by fundamental building blocks called repeating unit cells (RUC), such as shown in Figure 1. Considering a two-scale representation, the temperature field of an RUC resident in the material domain (Figure 1) can be expressed as

$$T(\boldsymbol{y}) = T^o(\boldsymbol{x}) + \tilde{T}(\boldsymbol{y}) \tag{6}$$

where T^o and $\tilde{T}$ stand for the macroscopic and fluctuating temperature contributions, respectively. Here, $\boldsymbol{y}$ indicates the local coordinates used in the RUC scale, whereas $\boldsymbol{x}$ represents the global coordinates for the RVE scale. Due to the material periodicity and the homogeneous boundary conditions imposed on the RVE, the fluctuation function $\tilde{T}(\boldsymbol{y})$ is periodic over the RUC domain.

Using Equation 6 and considering that $\boldsymbol{G}^o$ is a constant vector, the volume-averaged temperature gradient over the RUC volume Ω can be written as

$$\langle \boldsymbol{G} \rangle^{\Omega} = \boldsymbol{G}^o + \frac{1}{\Omega}\int_{\Omega} \tilde{\boldsymbol{G}}(\boldsymbol{y}) d\Omega \tag{7}$$

where the components of the fluctuating temperature gradient vector $\tilde{\boldsymbol{G}}$ are $\tilde{G}_i = \partial \tilde{T} / \partial y_i$.

Applying the divergence theorem to the integral appearing in Equation 7, the components of $\langle \boldsymbol{G} \rangle^{\Omega}$ can be expressed in the form

$$\langle G \rangle_i^{\Omega} = G_i^o + \frac{1}{\Omega}\int_{\Gamma} \tilde{T}(\boldsymbol{y}) n_i d\Gamma \tag{8}$$

being n_i the components of the outward unit vector normal to the RUC boundary surface Γ. As $\tilde{T}(\boldsymbol{y})$ is periodic on the RUC, the integral in Equation 8 must be null. Then,

$$\langle G \rangle_i^{\Omega} = G_i^o \tag{9}$$

i.e., the volume-averaged temperature gradient on the RUC is also equal to the temperature gradient of the homogeneous boundary conditions applied on the outer surface of the RVE. This is an important result for the solution of the homogenization problem focused in this work.

It is worth noting that even though Equation 9 is valid, the actual temperature boundary conditions of an RUC are different from those corresponding to the RVE, what can be justified by the periodic fluctuations $\tilde{T}(\boldsymbol{y})$ appearing in Equation 6. However, the homogenization problem can be solved considering that the response of the entire RVE under the above homogeneous temperature boundary conditions is identical to the response of an arbitrary RUC under appropriate periodic boundary conditions. This allows in general a great size reduction and simplification of the homogenization problem because the analysis involving the entire RVE can be substituted by other restricted to the domain of only one RUC. Those periodic boundary

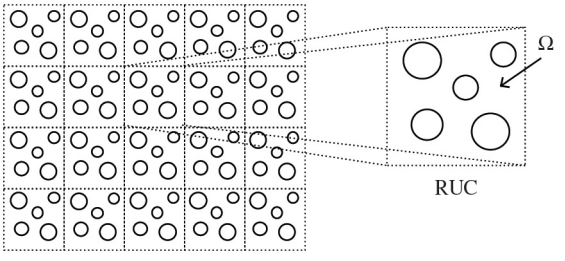

Figure 1. Periodic composite material and repeated unit cell (RUC).

conditions are imposed considering the same distribution of fluctuating temperature along the pairs of identical sides of the RUC characterized by the material periodicity.

3. Theoretical Formulation for the Unit Cell Homogenization

In this section the parametric finite-volume theory[7] is incorporated into the homogenization theory's framework based on a multiscale representation of the temperature field for evaluation of effective thermal conductivity in periodic unidirectional fiber reinforced composite. Here, the material unit cell can present arbitrary internal architectural arrangements of fibers coated by thin interphase with constant thickness and low thermal conductivity. As described in Section 3.3, the interphase subvolumes are replaced by interface elements with appropriate discontinuity in temperature and continuity in normal heat flux[13,14]. This procedure transforms the explicit three-phase problem (matrix, fiber and interphase) into a two-phase problem (matrix and fiber) with imperfect interfaces.

The parametric finite-volume theory already has been incorporated into the FVDAM's framework and successfully applied to the homogenization of elastic and elastic-plastic periodic composites materials with perfect interfaces[9-11].

In the parametric finite-volume formulation the actual material microstructure is discretized into quadrilateral subvolumes whose geometry and location are identified by their node coordinates. It is based on a mapping of a reference square in the parametric plane $\eta - \xi$ onto a quadrilateral subvolume in the Cartesian plane $y_2 - y_3$ of the actual material microstructure[7], as shown in Figure 2.

The mapping of the point (η, ξ) in the reference square to the corresponding point $(y_2 - y_3)$ in the quadrilateral subvolume of the actual discretized microstructure is expressed in the form

$$y_j(\eta,\xi) = N_1(\eta,\xi)\,y_{j,1} + N_2(\eta,\xi)\,y_{j,2} + N_3(\eta,\xi)\,y_{j,3} + N_4(\eta,\xi)\,y_{j,4} \quad (j=1,2) \tag{10}$$

where $y_{j,m}$ indicates the coordinate y_j of the subvolume node m and

$$N_1(\eta,\xi)=\frac{1}{4}(1-\eta)(1-\xi)\;\; N_2(\eta,\xi)=\frac{1}{4}(1+\eta)(1-\xi)$$
$$N_3(\eta,\xi)=\frac{1}{4}(1+\eta)(1+\xi)\;\; N_4(\eta,\xi)=\frac{1}{4}(1-\eta)(1+\xi) \tag{11}$$

3.1. Thermal conduction relations for a subvolume

For a homogeneous subvolume of the discretized RUC, the heat flux components are defined by the Fourier law

$$q_i = -k_{ij}\frac{\partial T}{\partial y_j} \qquad (i,j=1,2,3) \tag{12}$$

being k_{ij} the material thermal conductivities. Considering the temperature field given by Equation 6, this last equation becomes

$$q_i = -k_{ij}G_j^o - k_{ij}\frac{\partial \tilde{T}}{\partial y_j} \tag{13}$$

For the case of stationary thermal conduction without heat source and using Equation 13, the energy conservation equation is given by

$$\frac{\partial q_i}{\partial y_i} = -k_{ij}\frac{\partial^2 \tilde{T}}{\partial y_j^2} = 0 \tag{14}$$

Here, the fluctuating temperature field is assumed as independent of y_1 $(i.e., \partial\tilde{T}/\partial y_1 = 0)$ and approximated by a second-order representation in the local parametric coordinates[7]

$$\tilde{T}(\eta,\xi) = \tilde{T}_{00} + \eta\tilde{T}_{10} + \xi\tilde{T}_{01} + \frac{1}{2}\left(3\eta^2-1\right)\tilde{T}_{20} + \frac{1}{2}\left(3\xi^2-1\right)\tilde{T}_{02} \tag{15}$$

where $\tilde{T}_{mn}$ are unknown coefficients. For this second-order expansion, the surface-averaged values of the fluctuating temperature field on the subvolume faces (F_1, F_3) and (F_2, F_4), shown in Figure 2, are defined respectively by

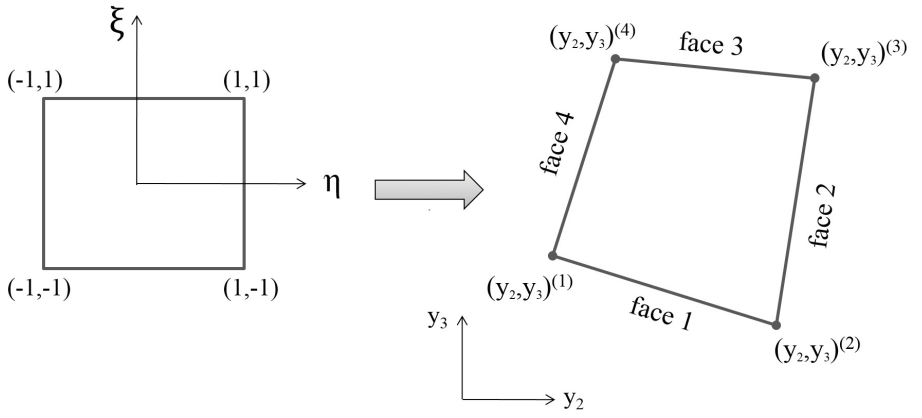

Figure 2. Mapping of the reference square subvolume onto a quadrilateral subvolume of the actual microstructure (after Cavalcante et al.[6]).

$$\bar{\tilde{T}}^{(1,3)} = \frac{1}{2}\int_{-1}^{+1} \tilde{T}\left(\eta, \xi = \mp 1\right) d\eta = \tilde{T}_{00} \mp \tilde{T}_{01} + \tilde{T}_{02}$$
$$\bar{\tilde{T}}^{(2,4)} = \frac{1}{2}\int_{-1}^{+1} \tilde{T}\left(\eta = \pm 1, \xi\right) d\xi = \tilde{T}_{00} \pm \tilde{T}_{10} + \tilde{T}_{20} \quad (16)$$

Using a similar definition for the surface-averaged gradients on the subvolume faces, the following expressions are easily obtained

$$\frac{\partial \bar{\tilde{T}}}{\partial \eta}^{(1,3)} = \tilde{T}_{10} \quad \frac{\partial \bar{T}}{\partial \xi}^{(1,3)} = \tilde{T}_{01} \pm 3\tilde{T}_{02}$$
$$\frac{\partial \bar{T}}{\partial \eta}^{(2,4)} = \tilde{T}_{10} \pm 3\tilde{T}_{20} \quad \frac{\partial \bar{T}}{\partial \xi}^{(2,4)} = \tilde{T}_{01} \quad (17)$$

In the context of the parametric finite-volume theory, the relation between surface-averaged gradients on the *p* th face of a subvolume in the reference and actual coordinate systems is simplified by using the volume-averaged Jacobian $\bar{\boldsymbol{J}}$, as follows:

$$\begin{bmatrix} \frac{\partial \bar{\tilde{T}}}{\partial y_2} \\ \frac{\partial \bar{\tilde{T}}}{\partial y_3} \end{bmatrix}^{(p)} = \hat{\boldsymbol{J}} \begin{bmatrix} \frac{\partial \bar{\tilde{T}}}{\partial \eta} \\ \frac{\partial \bar{\tilde{T}}}{\partial \xi} \end{bmatrix}^{(p)} \quad (18)$$

where $\hat{\boldsymbol{J}}^{-1} = \bar{\boldsymbol{J}} = \frac{1}{4}\int_{-1-1}^{+1+1} \boldsymbol{J} d\eta d\xi$, being

$$\boldsymbol{J} = \begin{bmatrix} \frac{\partial y_2}{\partial \eta} & \frac{\partial y_3}{\partial \eta} \\ \frac{\partial y_2}{\partial \xi} & \frac{\partial y_3}{\partial \xi} \end{bmatrix} \quad (19)$$

Taking into account Equations 13 and 18, the relation between the surface-averaged heat flux vector and the surface-averaged temperature gradient vector for the *p* th face can be written in the form

$$\hat{\boldsymbol{q}}^{(p)} = \begin{bmatrix} \hat{q}_2 \\ \hat{q}_3 \end{bmatrix}^{(p)} = \bar{\boldsymbol{k}} \begin{bmatrix} G_2^o \\ G_3^o \end{bmatrix} + \bar{\boldsymbol{k}}\hat{\boldsymbol{J}} \begin{bmatrix} \frac{\partial \bar{\tilde{T}}}{\partial \eta} \\ \frac{\partial \bar{\tilde{T}}}{\partial \xi} \end{bmatrix}^{(p)} \quad (20)$$

with $\bar{\boldsymbol{k}} = -\begin{bmatrix} k_{22} & k_{23} \\ k_{23} & k_{33} \end{bmatrix}$.

Based on Equation 20, the total surface-averaged heat flux vector for the *p* th face of the subvolume can be expressed as $\bar{\tilde{\boldsymbol{q}}}^{(p)} = \boldsymbol{q}^o + \hat{\tilde{\boldsymbol{q}}}^{(p)}$, where $\boldsymbol{q}^o$ is the constant macroscopic part depending on the known values G_k^o $(k = 2,3)$ and $\hat{\tilde{\boldsymbol{q}}}^{(p)}$ indicates the unknown contribution of the surface-averaged fluctuating temperature gradients.

The projection of the surface-averaged heat flux onto the normal to the *p* th face of the subvolume is given by

$$\hat{q}_n^{(p)} = \boldsymbol{n}^{(p)}\hat{\boldsymbol{q}}^{(p)} = \boldsymbol{n}^{(p)}\bar{\boldsymbol{k}} \begin{bmatrix} G_2^o \\ G_3^o \end{bmatrix} + \boldsymbol{n}^{(p)}\bar{\boldsymbol{k}}\hat{\boldsymbol{J}} \begin{bmatrix} \frac{\partial \bar{\tilde{T}}}{\partial \eta} \\ \frac{\partial \bar{\tilde{T}}}{\partial \xi} \end{bmatrix}^{(p)} \quad (21)$$

where $\boldsymbol{n}^{(p)} = \begin{bmatrix} n_2 & n_3 \end{bmatrix}^{(p)}$, with n_2 and n_3 indicating the components of the outward unit vector normal to the face.

3.2. Local thermal conductivity matrix of a subvolume

In this subsection is presented the derivation of the local thermal conductivity matrix for a subvolume of a discretized RUC domain. Herein, this conductivity matrix relates the surface-averaged fluctuating temperatures to the normal surface-averaged fluctuating heat fluxes associated with the four faces of the subvolume. Introducing Equation 17 into Equation 21 for each face *p*, the normal surface-averaged heat flux vector for the subvolume can be obtained in the form

$$\begin{bmatrix} \hat{q}_n^{(1)} \\ \hat{q}_n^{(2)} \\ \hat{q}_n^{(3)} \\ \hat{q}_n^{(4)} \end{bmatrix} = \begin{bmatrix} \boldsymbol{n}^{(1)} \\ \boldsymbol{n}^{(2)} \\ \boldsymbol{n}^{(3)} \\ \boldsymbol{n}^{(4)} \end{bmatrix} \bar{\boldsymbol{k}} \begin{bmatrix} G_2^o \\ G_3^o \end{bmatrix} + \begin{bmatrix} \boldsymbol{v}^{(1)} \\ \boldsymbol{v}^{(2)} \\ \boldsymbol{v}^{(3)} \\ \boldsymbol{v}^{(4)} \end{bmatrix} \begin{bmatrix} \tilde{T}_{10} \\ \tilde{T}_{01} \\ \tilde{T}_{20} \\ \tilde{T}_{02} \end{bmatrix} \quad (22)$$

where $\boldsymbol{v}^{(p)} = \boldsymbol{n}^{(p)}\bar{\boldsymbol{k}}\hat{\boldsymbol{J}}\boldsymbol{a}^{(p)}$ and

$$\boldsymbol{a}^{(1,3)} = \begin{bmatrix} 1 & 0 & 0 & 0 \\ 0 & 1 & 0 & \mp 3 \end{bmatrix} \quad \boldsymbol{a}^{(2,4)} = \begin{bmatrix} 1 & 0 & \pm 3 & 0 \\ 0 & 1 & 0 & 0 \end{bmatrix} \quad (23)$$

The next step consists of obtaining a relation between the unknown temperature coefficients appearing in Equation 22 and the fluctuating surface-averaged temperatures on the subvolume faces. For this, Equation 16 are used together with the volume-averaged heat conduction equation for the subvolume. This last equation is obtained from Equation 14 using the inverse of the volume-averaged Jacobian, $\hat{\boldsymbol{J}}$, to derive the relationships between the second partial derivatives of the fluctuating temperature with respect to (y_2, y_3) coordinates and the corresponding second derivatives with respect to (η, ξ) coordinates. The volume-averaged heat conduction equation resulting of that procedure can be written as

$$\left(k_{22}\hat{J}_{11}^2 + 2k_{23}\hat{J}_{11}\hat{J}_{21} + k_{33}\hat{J}_{21}^2\right)\tilde{T}_{20} + \left(k_{22}\hat{J}_{12}^2 + 2k_{23}\hat{J}_{12}\hat{J}_{22} + k_{33}\hat{J}_{22}^2\right)\tilde{T}_{02} = 0 \quad (24)$$

Now, using Equations 16 and 24, the zero *th* order coefficient $\tilde{T}_{00}$ is obtained directly in function of the surface-averaged fluctuating temperatures as

$$\tilde{T}_{00} = \lambda\left(\bar{\tilde{T}}^{(2)} + \bar{\tilde{T}}^{(4)}\right) + \omega\left(\bar{\tilde{T}}^{(1)} + \bar{\tilde{T}}^{(3)}\right) \quad (25)$$

where, for the case of isotropic material with $k_{22} = k_{33} = k$ and $k_{23} = 0$,

$$\lambda = \frac{\hat{J}_{11}^2 + \hat{J}_{21}^2}{2\left(\hat{J}_{11}^2 + \hat{J}_{12}^2 + \hat{J}_{21}^2 + \hat{J}_{22}^2\right)} \quad \omega = \frac{\hat{J}_{12}^2 + \hat{J}_{22}^2}{2\left(\hat{J}_{11}^2 + \hat{J}_{12}^2 + \hat{J}_{21}^2 + \hat{J}_{22}^2\right)} \quad (26)$$

Substituting Equation 25 into Equation 16, the relation between the coefficients of the fluctuating temperature field and the fluctuating surface-averaged temperatures on the subvolume faces is found in the form

$$\begin{bmatrix} \tilde{T}_{10} \\ \tilde{T}_{01} \\ \tilde{T}_{20} \\ \tilde{T}_{02} \end{bmatrix} = \begin{bmatrix} 0 & 1/2 & 0 & -1/2 \\ -1/2 & 0 & 1/2 & 0 \\ -\omega & 1/2-\lambda & -\omega & 1/2-\lambda \\ 1/2-\omega & -\lambda & 1/2-\omega & -\lambda \end{bmatrix} \begin{bmatrix} \bar{\tilde{T}}^{(1)} \\ \bar{\tilde{T}}^{(2)} \\ \bar{\tilde{T}}^{(3)} \\ \bar{\tilde{T}}^{(4)} \end{bmatrix} = \boldsymbol{B} \begin{bmatrix} \bar{\tilde{T}}^{(1)} \\ \bar{\tilde{T}}^{(2)} \\ \bar{\tilde{T}}^{(3)} \\ \bar{\tilde{T}}^{(4)} \end{bmatrix} \quad (27)$$

Introducing Equation 27 in Equation 22, the normal surface-averaged heat flux vector for the subvolume becomes

$$\begin{bmatrix} \hat{q}_n^{(1)} \\ \hat{q}_n^{(2)} \\ \hat{q}_n^{(3)} \\ \hat{q}_n^{(4)} \end{bmatrix} = \begin{bmatrix} \boldsymbol{n}^{(1)} \\ \boldsymbol{n}^{(2)} \\ \boldsymbol{n}^{(3)} \\ \boldsymbol{n}^{(4)} \end{bmatrix} \bar{\boldsymbol{k}} \begin{bmatrix} G_2^o \\ G_3^o \end{bmatrix} + \begin{bmatrix} \boldsymbol{v}^{(1)} \\ \boldsymbol{v}^{(2)} \\ \boldsymbol{v}^{(3)} \\ \boldsymbol{v}^{(4)} \end{bmatrix} \boldsymbol{B} \begin{bmatrix} \bar{\tilde{T}}^{(1)} \\ \bar{\tilde{T}}^{(2)} \\ \bar{\tilde{T}}^{(3)} \\ \bar{\tilde{T}}^{(4)} \end{bmatrix} \quad (28)$$

which can be written in compact form as,

$$\hat{\boldsymbol{q}}_n = \boldsymbol{N}\bar{\boldsymbol{k}}\boldsymbol{G}^{\boldsymbol{o}} + \boldsymbol{K}_L \bar{\tilde{\boldsymbol{T}}} \quad (29)$$

where $\boldsymbol{G}^{\boldsymbol{o}} = \begin{bmatrix} G_2^o \\ G_3^o \end{bmatrix}$ and the local conductivity matrix of the subvolume is

$$\boldsymbol{K}_L = \boldsymbol{V}\boldsymbol{B} \quad (30)$$

with $\boldsymbol{V} = \begin{bmatrix} \boldsymbol{v}^{(1)} & \boldsymbol{v}^{(2)} & \boldsymbol{v}^{(3)} & \boldsymbol{v}^{(4)} \end{bmatrix}^T$.

3.3. Imperfect interface element

Figure 3a shows an arbitrarily curved thin interphase of constant thickness *h* located between a fiber and the matrix of a composite material. It is shown in Benveniste[14] that the mentioned thin interphase can be approximately replaced by an equivalent interface, positioned at the location of the middle surface S_0, considering appropriate conditions of temperature and normal heat flux for the case of thermal analysis (Figure 3b). Using a Taylor expansion, Hashin[13] showed that a thin interphase with much smaller thermal conductivity than the phases can produce a finite jump in the temperature while a finite jump in the normal heat flux can be produced when the interphase thermal conductivity is very large.

Based on these results, in the present work the thin slowly conducting interphase is represented by an interface lying between the fiber and the matrix, across which the temperature exhibits a discontinuity whereas the normal heat flux presents continuity. For the case of isotropic and homogeneous interphase, the temperature jump across the interface can be written as follows[14]:

$$T_+ - T_- = \frac{h}{2}\left(\frac{1}{k_m} + \frac{1}{k_f} - \frac{2}{k_I}\right) q_n \quad (31)$$

where T_+ and T_- are the temperatures at the interface S_0 on the sides of the matrix and fiber respectively (Figure 3b). The parameters k_m, k_f and k_I stand for the thermal conductivities of the matrix, fiber and interphase, respectively. In Equation 31, q_n indicates the heat flux normal to the interface assumed as positive in the direction shown in Figure 3b.

Considering Equation 6 and taking into account that the macroscopic temperature jump $T_+^0 - T_-^0$ across the interface is null, Equation 31 can be written as

$$\tilde{T}_+ - \tilde{T}_- = \frac{h}{2}\left(\frac{1}{k_m} + \frac{1}{k_f} - \frac{2}{k_I}\right) q_n \quad (32)$$

being $\tilde{T}_+$ and $\tilde{T}_-$ the interfacial fluctuating temperatures on the sides of the matrix and fiber, respectively.

As the parametric finite-volume formulation employs quadrilateral subvolumes for discretization of fiber and matrix, the interfaces are discretized into straight line segments, as shown in Figure 4. Using Equation 32, the surface-averaged temperature jump across an interface element is given by

$$\bar{\tilde{T}}_2 - \bar{\tilde{T}}_1 = \frac{h}{2}\left(\frac{1}{k_m} + \frac{1}{k_f} - \frac{2}{k_I}\right) \hat{q}_n \quad (33)$$

where $\bar{\tilde{T}}_1$ and $\bar{\tilde{T}}_2$ are the surface-averaged fluctuating temperatures on the element faces F_1 and F_2, respectively, and $\hat{q}_n$ is the surface-averaged normal heat flux across the interface element. For the interface element, the relation between the surface-averaged normal heat fluxes on the faces F_1 and F_2 is given by $\hat{q}_n^{(1)} = -\hat{q}_n^{(2)} = -\hat{q}_n$. Then, through Equation 33, the following expression is derived

$$\hat{q}_n^{(1)} = -\hat{q}_n^{(2)} = c\left(\bar{\tilde{T}}_2 - \bar{\tilde{T}}_1\right) \quad (34)$$

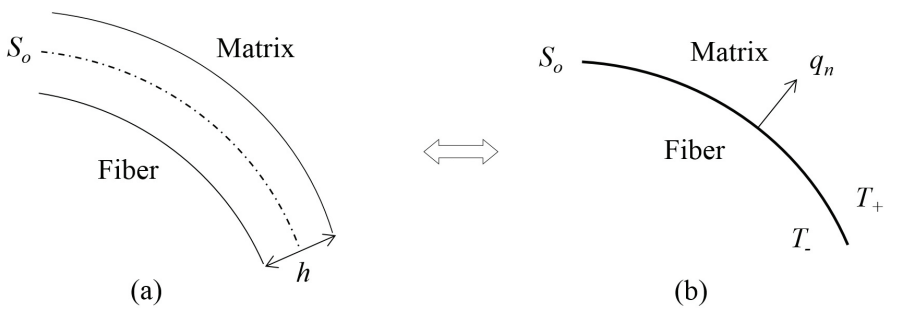

Figure 3. (a) Interphase fiber/matrix and (b) equivalent imperfect interface.

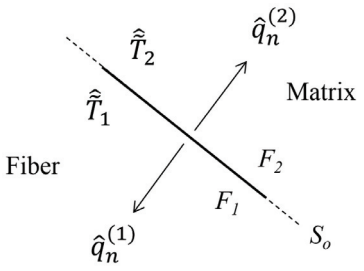

Figure 4. Interface element.

where

$$c = \frac{2}{h}\frac{1}{\frac{1}{k_m}+\frac{1}{k_f}-\frac{2}{k_I}} \tag{35}$$

Equation 34 can be written in a matrix form as

$$\begin{Bmatrix} \hat{q}_n^{(1)} \\ \hat{q}_n^{(2)} \end{Bmatrix} = \begin{bmatrix} c & -c \\ -c & c \end{bmatrix} \begin{Bmatrix} \hat{\bar{\bar{T}}}_1 \\ \hat{\bar{\bar{T}}}_2 \end{Bmatrix} \tag{36}$$

Then, the local conductivity matrix of the interface element is given by

$$K_{LI} = \begin{bmatrix} c & -c \\ -c & c \end{bmatrix} \tag{37}$$

3.4. Global conductivity matrix construction

The normal surface-averaged heat fluxes on the local faces of each subvolume and interface elements of the unit cell are related to the corresponding surface-averaged fluctuating temperatures through the local conductivity matrix, as shown in Equations 29 and 36. The local conductivity matrices are assembled into a global system of equations by applying surface-averaged interfacial fluctuating temperature and normal heat flux compatibility conditions, followed by the specified boundary conditions. This approach is based on an appropriate global face numbering system, in which each internal local face has a corresponding global face number, common to the adjacent subvolumes or subvolume and interface element, while the external faces of subvolumes along the opposite unit cell boundaries are numbered taking into account the periodicity conditions. These external faces, with similar fluctuating temperature distributions imposed by the periodicity conditions, receive common face numbers. The procedure for assembling the global system is similar to that used in the finite-element algorithms. In these later, the degrees of freedom are associated with the element nodes, while in the present finite-volume formulation they are referred to the subvolume and interface element faces.

Imposing compatibility conditions of normal surface-averaged heat flux and surface-averaged fluctuating temperatures on the common interfaces, as well as, the specified boundary conditions, the global system of equations takes the form

$$\boldsymbol{K_G}\tilde{\boldsymbol{T}}_{\boldsymbol{G}} = \boldsymbol{Q}_{\boldsymbol{G}}^{0} \tag{38}$$

where $\boldsymbol{K_G}$ is the global conductivity matrix and $\boldsymbol{Q}_{\boldsymbol{G}}^{0}$ is a vector comprised of the resulting macroscopic normal surface-averaged fluxes in the interfaces of adjacent subvolumes and faces located along the discretized unit cell boundary. The vector $\tilde{\boldsymbol{T}}_{\boldsymbol{G}}$ contains all the unknown interfacial and boundary surface-averaged fluctuating temperatures. As the matrix $\boldsymbol{K_G}$ is singular, the solution of Equation 38 is not directly accessible. This problem can be eliminated by imposing null surface-averaged fluctuating temperatures on the four corner subvolume faces. The remaining surface-averaged fluctuating temperatures are determined by solving the reduced system of equations.

3.5. Homogenized conductivity matrix

The in-plane homogenized Fourier law for the composite material relates the effective heat flux $\boldsymbol{Q}^*$ to the macroscopic temperature gradient $\boldsymbol{G}^0$ as follows:

$$\boldsymbol{Q}^* = -\boldsymbol{K}^*\boldsymbol{G}^{\boldsymbol{o}} \tag{39}$$

where $\boldsymbol{Q}^* = \begin{bmatrix} Q_2^* & Q_3^* \end{bmatrix}^T$ and $\boldsymbol{K}^*$ is the effective thermal conductivity. The effective heat flux is defined as the volume average of the in-plane heat flux field $\boldsymbol{q}$ throughout the repeating unit cell by

$$\boldsymbol{Q}^* = \frac{1}{\Omega}\left[\int_{\Omega_m} \boldsymbol{q}(y_2,y_3)\,d\Omega_m + \int_{\Omega_f} \boldsymbol{q}(y_2,y_3)\,d\Omega_f + \int_{\Omega_I} \boldsymbol{q}(y_2,y_3)\,d\Omega_I\right] \tag{40}$$

where Ω_m, Ω_f and Ω_I denote the matrix, fiber and interphase domains, respectively. Using the Fourier law (Equation 12) and assuming homogeneous and isotropic phases, Equation 40 can be rewritten in the form

$$\boldsymbol{Q}^* = -\frac{1}{\Omega}\left[k_m \int_{\Omega_m} \boldsymbol{G}(y_2,y_3)\,d\Omega_m + k_f \int_{\Omega_f} \boldsymbol{G}(y_2,y_3)\,d\Omega_f + k_I \int_{\Omega_I} \boldsymbol{G}(y_2,y_3)\,d\Omega_I\right] \tag{41}$$

being $\boldsymbol{G}$ the local temperature gradient vector. After the substitution of the interphases by the imperfect interfaces and discretization of the unit cell, the following approximation can be used to evaluate the effective heat flux

$$\boldsymbol{Q}^* \cong -\sum_{l=1}^{N_m} k_m \bar{\upsilon}_m^{(l)} \hat{\boldsymbol{G}}_m^{(l)} - \sum_{r=1}^{N_f} k_f \bar{\upsilon}_f^{(r)} \hat{\boldsymbol{G}}_f^{(r)} - \sum_{s=1}^{N_I} \frac{\upsilon_I^{(s)}}{2}\left[(k_I - k_m)\hat{\boldsymbol{G}}_{Im}^{(s)} + (k_I - k_f)\hat{\boldsymbol{G}}_{If}^{(s)}\right] \tag{42}$$

where N_m and N_f indicate the number of subvolumes used in the discretization of the matrix and fiber domains and N_I is the number of interface elements. The symbols $\bar{\upsilon}_m^{()}$ and $\bar{\upsilon}_f^{()}$ are the volume fractions of the matrix and fiber subvolumes over the discretized unit cell with interphase replaced by interface and $\upsilon_I^{()}$ are the volume fractions of the interphase elements, respectively. In Equation 42, $\hat{\boldsymbol{G}}_m^{()}$ and $\hat{\boldsymbol{G}}_f^{()}$ are the volume-averaged temperature gradients of the matrix and fiber subvolumes, while $\hat{\boldsymbol{G}}_{Im}^{()}$ and $\hat{\boldsymbol{G}}_{If}^{()}$ indicate the surface-averaged temperature gradients evaluated on the sides of matrix and fiber of each interface element, respectively. Equation 42 takes into account that to replace an interphase by an imperfect interface both the matrix and fiber materials are extended of $h/2$ up to that interface.

Now, introducing the concept of subvolume (or interface element) temperature gradient concentration matrix $\boldsymbol{H}^{()}$, such that,

$$\hat{\boldsymbol{G}}_m^{(l)} = \boldsymbol{H}_m^{(l)}\boldsymbol{G}^o \;\; \hat{\boldsymbol{G}}_f^{(r)} = \boldsymbol{H}_f^{(r)}\boldsymbol{G}^o \;\; \hat{\boldsymbol{G}}_{lm}^{(s)} = \boldsymbol{H}_{lm}^{(s)}\boldsymbol{G}^o \;\; \hat{\boldsymbol{G}}_{lf}^{(s)} = \boldsymbol{H}_{lf}^{(s)}\boldsymbol{G}^o \quad (43)$$

into Equation 42 and using Equation 39, the following relation is found for the homogenized thermal conductivity

$$\boldsymbol{K}^* = \sum_{l=1}^{N_m} k_m \overline{\upsilon}_m^{(l)} \boldsymbol{H}_m^{(l)} + \sum_{r=1}^{N_f} k_f \overline{\upsilon}_f^{(r)} \boldsymbol{H}_f^{(r)} + \sum_{s=1}^{N_I} \frac{\upsilon_f^{(s)}}{2} \left[\left(k_I - k_m\right) \boldsymbol{H}_{lm}^{(s)} + \left(k_I - k_f\right) \boldsymbol{H}_{lf}^{(s)} \right] \quad (44)$$

The 2×2 matrices $\boldsymbol{H}^{(\,)}$ appearing in Equation 44 can be readily obtained through the solutions of Equation 38 corresponding to two conveniently selected macroscopic gradient $\boldsymbol{G}^o$. For each assumed $\boldsymbol{G}^o$, Equation 38 provides the fluctuating surface-averaged temperatures, what enables the evaluation of the temperature gradient field inside each subvolume or interface element and, then, the vectors $\hat{\boldsymbol{G}}^{(\,)}$ can be readily determined. As example, for $\boldsymbol{G}^o = [1 \quad 0]^T$, Equations 43 provide, for a matrix or fiber subvolume, $H_{22}^{(\,)} = \hat{G}_2^{(\,)}$ and $H_{32}^{(\,)} = \hat{G}_3^{(\,)}$, whereas for $\boldsymbol{G}^o = [0 \quad 1]^T$, the same equations give $H_{23}^{(\,)} = \hat{G}_2^{(\,)}$ and $H_{33}^{(\,)} = \hat{G}_3^{(\,)}$.

4. Numerical Examples

4.1. Unidirectional two-phase composite with square and hexagonal arrays of fibers

This first example consists of a unidirectional two-phase composite material with periodic square and hexagonal distributions of fibers (Figure 5). The assumption of perfect fiber-matrix interfaces is adopted for this case. Here, the objective is to investigate the effect of the RUC discretization on the effective thermal conductivity, as well as, to illustrate the results obtained by the present formulation compared with finite-element solutions for a wide range of fiber-volume fractions and fiber-to-matrix thermal conductivity ratios.

For the unit cell discretization convergence study, three different meshes for each type of fiber array are used, as shown in Figure 6 for a fiber-volume fraction of 0.60. Figures 7 and 8 show the results of the effective transverse thermal conductivity $K^* = K_{22}^* = K_{33}^*$, normalized by k_m, in function of the conductivity ratio k_f / k_m, for the RUC discretizations illustrated in Figure 6.

Results obtained by Sihn and Roy[6], using the finite-element method, are also presented in Figures 7 and 8. Figure 9 shows the results for the normalized effective transverse thermal conductivity of the composite for a large range of fiber volume fraction, considering a fiber-to-matrix thermal conductivity ratio $k_f / k_m = 666$. In addition to the solutions obtained by Sihn and Roy[6], experimental results due to Thornburg and Pears[1] are also presented in Figure 9. It is observed that the results provided by the proposal model exhibit fast convergence with the RUC mesh refinement and a very good agreement with the finite-element solutions.

4.2. Size-dependence of the effective thermal conductivity of a composite with interfacial thermal resistance

In this example, the proposal model is applied to investigate the effect of the fiber size on the effective thermal conductivity for a composite SiC/Al with interfacial thermal resistance and periodic square fiber distribution. The thermal conductivities of the matrix and fibers are assumed as $k_m = 178 W/mK$ and $k_f = 300 W/mK$, respectively.

The interphases have thickness $h = 20nm$ and thermal conductivity $k_I = 2.918 W/mK$.

A fiber-volume fraction of 30% is assumed for the composite. Figure 10 shows the variation of the normalized effective thermal conductivity with the fiber radius ($0.05\mu m \leq r \leq 10\mu m$), considering three conditions: a) three-phase material (matrix, fiber and interphase) with perfect interfaces, b) two-phase material (matrix and fiber) with imperfect interfaces and c) two-phase material (matrix and fiber) with perfect interfaces. To verify the model, the numerical results are compared with those obtained by an analytical micromechanics formulation presented in Nan et al.[15], which predicts the effective thermal conductivity of composite materials with interfacial thermal resistance in terms of an effective medium approach combined with the essential concept of Kapitza thermal contact resistance. Figure 10 clearly shows the great fiber size-dependence effect on the effective thermal conductivity (Kapitza effect) for small radius values and also a very good agreement of the results obtained by the presented model, incorporating the imperfect interface elements, in comparison with those predicted using three-phase unit cells with perfect interfaces, as well as, with the analytical micromechanics solution[15]. The difference between the result for two-phase unit cell without interphase (horizontal dashed line) and the other curves in Figure 10 represents the influence of the presence of the thin interphase on the effective thermal conductivity of the composite material, which decreases as the fiber size increases.

4.3. Analysis of applicability of the assumption of imperfect interface with continuity in normal heat flux and discontinuity in temperature

The aim of this example is to investigate the range of the interphase thermal conductivity k_i for which the usual assumption of imperfect interface with continuity in normal heat flux and discontinuity in temperature can be successfully employed. For this, a periodic composite with unidirectional circular fibers coated by thin interphases is considered. The fibers have a radius $r = 1\mu m$ and square periodic array. The thermal conductivity of the matrix is assumed as $k_m = 1 W/mK$. Two situations are considered: a) the unit cell is discretized and analyzed as composed

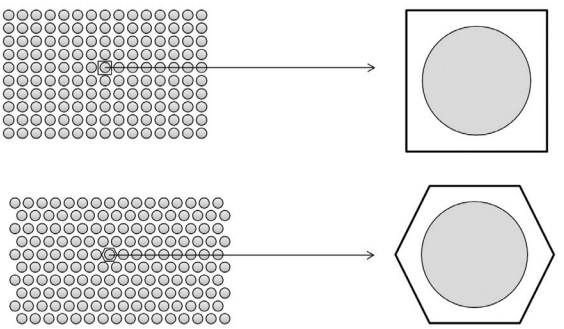

Figure 5. Unidirectional two-phase composite with periodic square and hexagonal distributions of fibers.

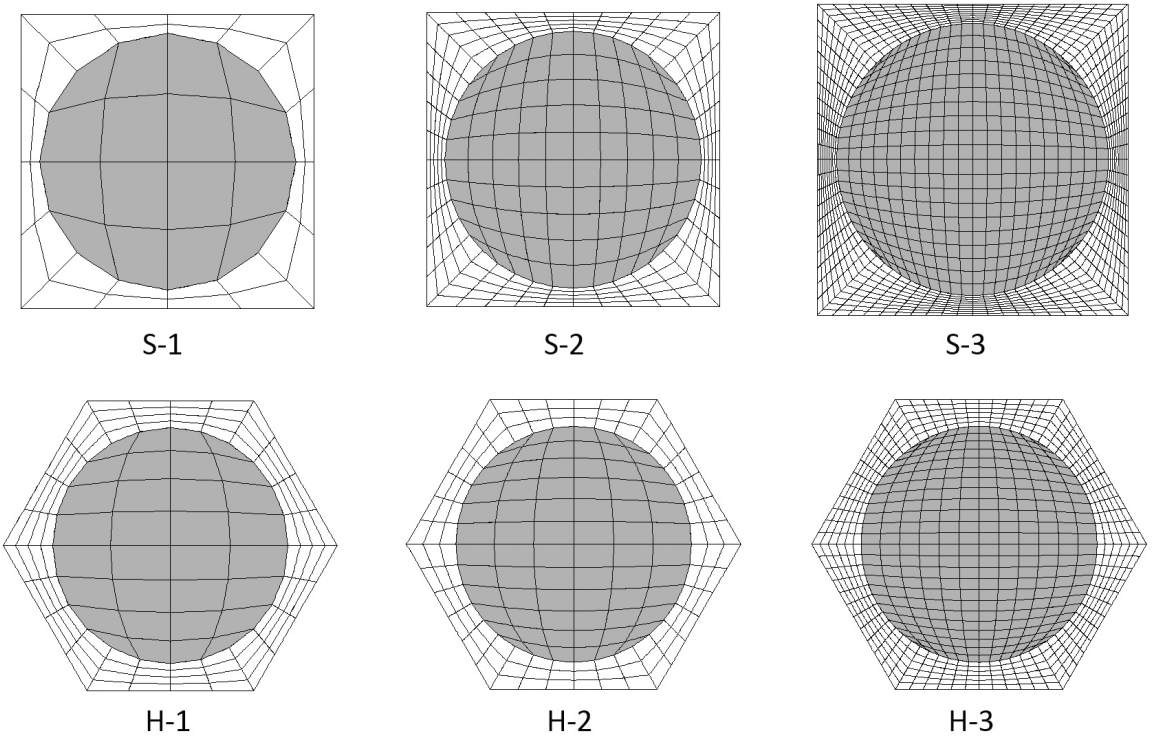

Figure 6. RUC discretizations for square and hexagonal arrays.

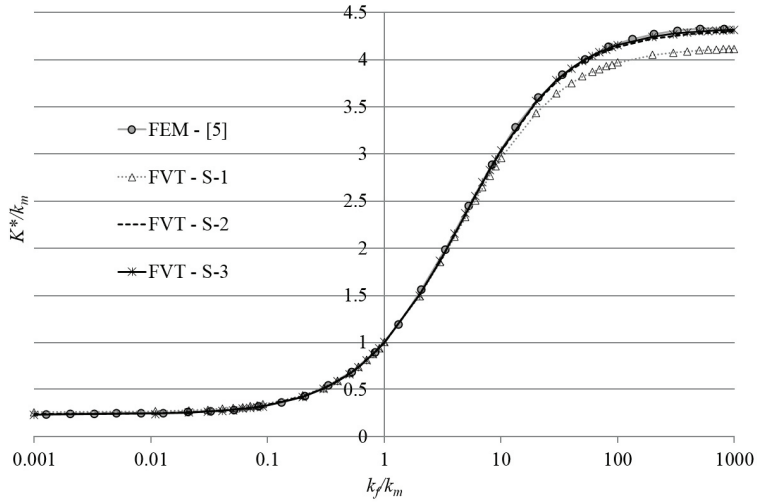

Figure 7. Normalized effective transverse thermal conductivity of the composite with square distribution of fibers.

by three phases (matrix, fiber and interphase) with perfect interfaces e b) the unit cell is discretized and analyzed as a two-phase material with imperfect interfaces. In this last situation, the actual interphase is replaced by an interface with continuous normal heat flux and discontinuous temperature field. For the first situation the interfaces matrix-interphase and interphase-fiber are considered as perfect, i.e., with continuity in both normal heat flux and temperature. Figures 11, 12 and 13 show the results obtained for fiber-volume fractions of 30%, 50% and 70%, respectively. For each fiber-volume fraction, four different ratios k_m / k_f (0.02, 1, 10 and 50) are considered. In the comparative analyses of this example, the solutions obtained for the cases of three-phase material with perfect interfaces are taken as reference to evaluate the results generated using the imperfect interface model.

For all analyzed cases, it is observed that the thermal conductivity of the connected matrix phase has a strong influence on the effective thermal conductivity. This occurs because to reach the disconnected fiber phase the heat must be transported through the connected matrix phase. The results show a continuous reduction of the effective

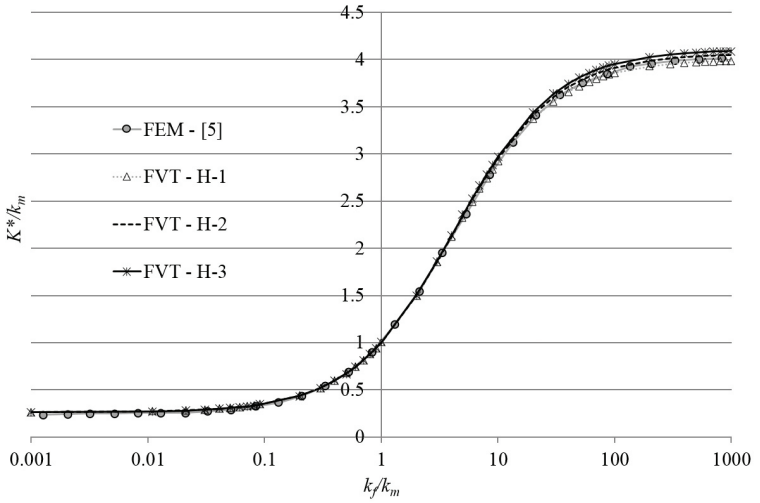

Figure 8. Normalized effective transverse thermal conductivity of the composite with hexagonal distribution of fibers.

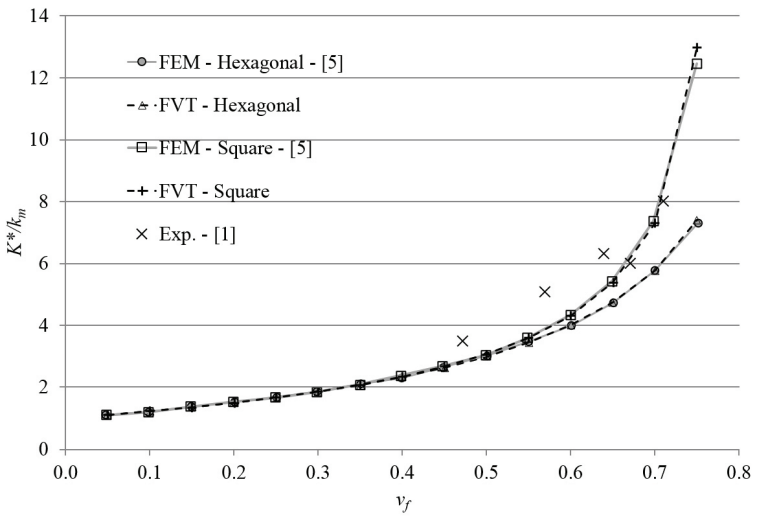

Figure 9. Variation of the normalized effective transverse thermal conductivity of the composite in function of the fiber volume fraction.

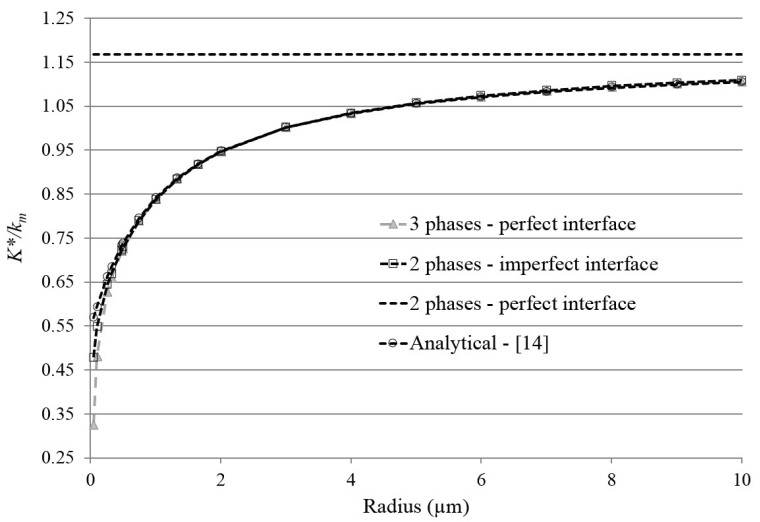

Figure 10. Variation of the effective thermal conductivity with the fiber radius.

thermal conductivity with the decrease of the interphase thermal conductivity. However, when $k_f > k_m$ the values of the effective thermal conductivity remain practically constant for $k_i > k_m$ as shown in Figures 11a, b, 12a, b and 13a, b for the cases of three-phase materials with perfect interfaces. On the other hand, when the matrix is more conducting than the fibers ($k_m > k_f$), the results show that the effective thermal conductivity present significant augment with the increase of the interphase thermal conductivity in the interval $k_i > k_m$. This happen because the interphase is more conducting than

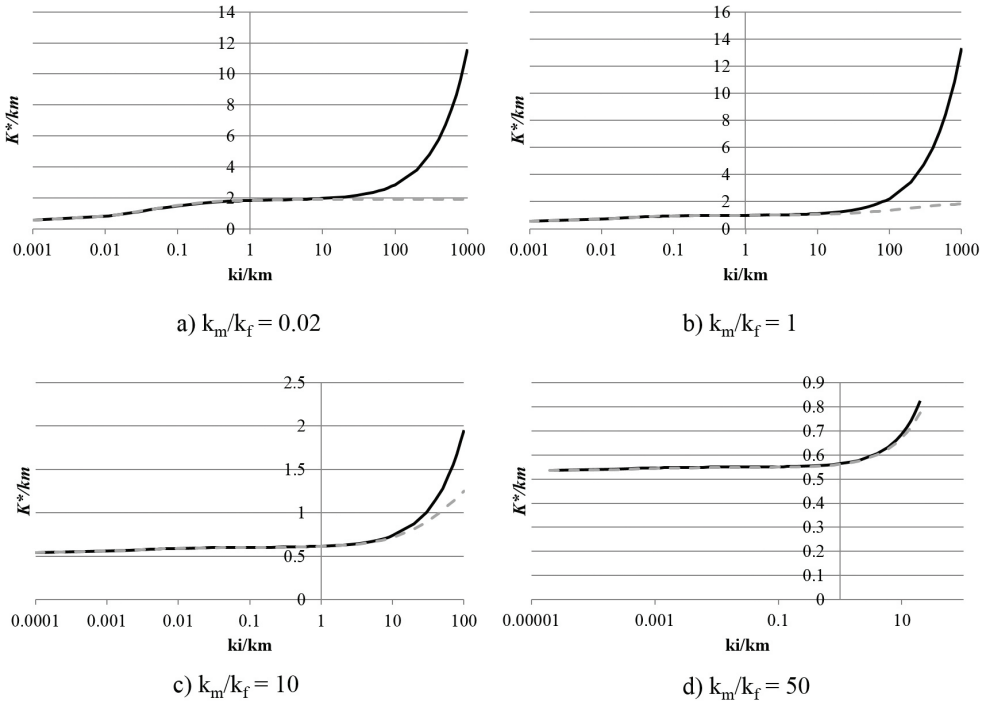

Figure 11. Effective thermal conductivity versus interphase thermal conductivity for imperfect/perfect interfaces and v_f = 30% (solid lines - imperfect interfaces; dashed lines - perfect interfaces).

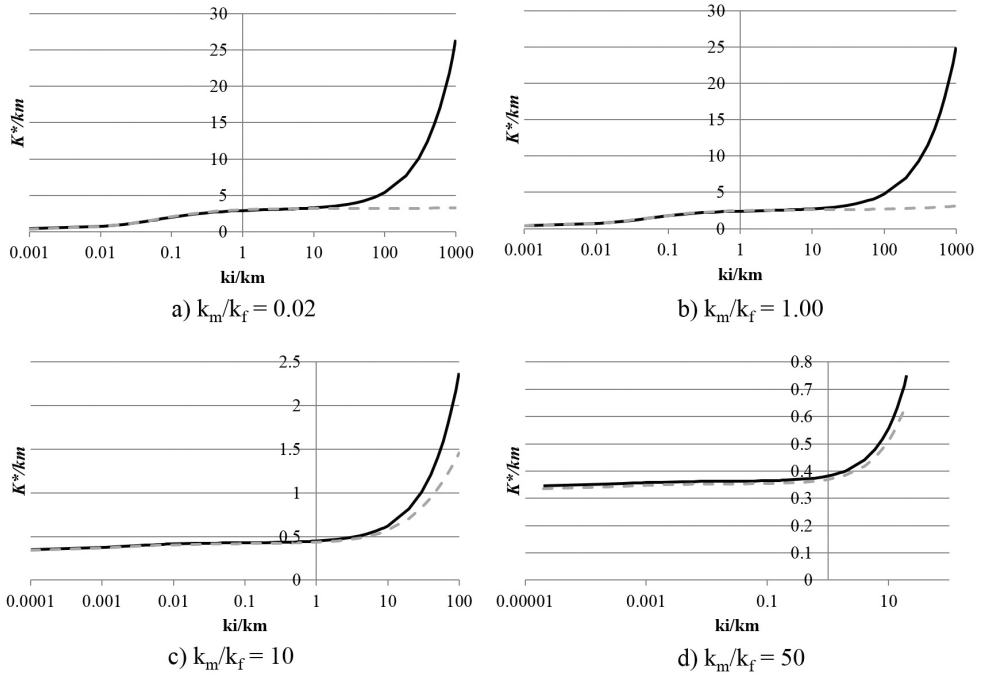

Figure 12. Effective thermal conductivity versus interphase thermal conductivity for imperfect/perfect interfaces and v_f = 50% (solid lines - imperfect interfaces; dashed lines - perfect interfaces).

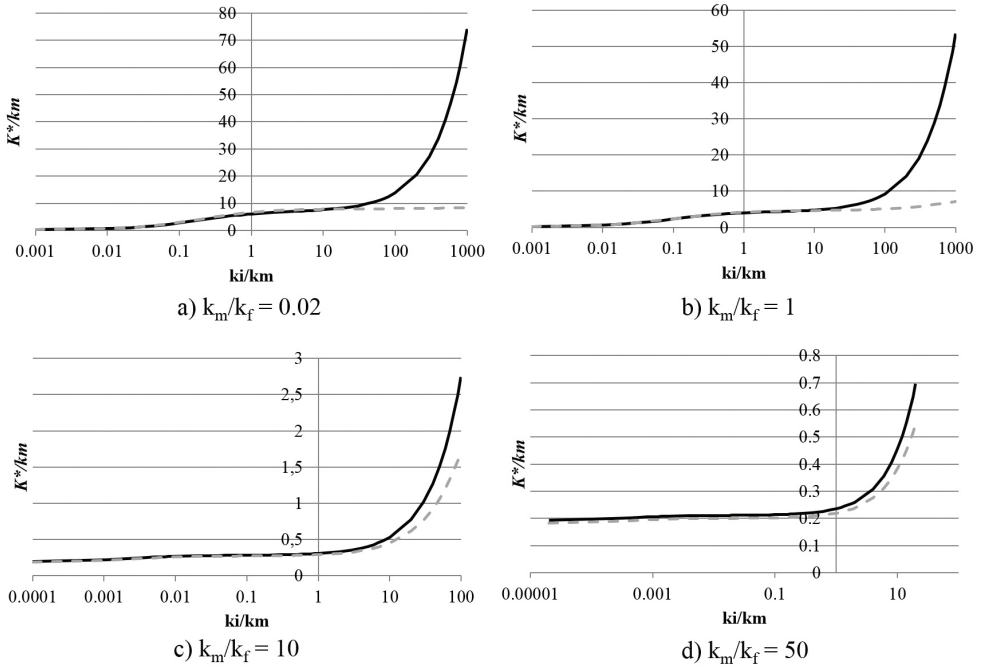

Figure 13. Effective thermal conductivity versus interphase thermal conductivity for imperfect/perfect interfaces and $v_f = 70\%$ (solid lines - imperfect interfaces; dashed lines - perfect interfaces).

the matrix, which has a thermal conductivity $k_m > k_f$. In this last case, it is also observed lower differences between the curves corresponding to the assumptions of three-phase material with perfect interfaces and two-phase material with imperfect interface, respectively, in the range $k_i > k_m$. When the fiber-volume fraction increases, the volume of interphase inside a unit cell is augmented and, as a consequence, the influence of k_i on the effective thermal conductivity K^* is increased, what is responsible for the greater slope of the curve $K^* > k_m$ for $k_i > k_m$. (Figures 11c, d, 12c, d and 13c, d).

Figures 11, 12 and 13 show that the curves obtained with the above two assumptions are practically coincident in the interval $k_i \leq k_m$. The results also allow to conclude that the proposed model of imperfect interfaces can provide good results for ratio k_i / k_m smaller than a limit $(k_i / k_m)_{lim}$. As it can be seen in Figures 11, 12 and 13, this limit is greater than 10 for the most of the analyzed cases.

5. Conclusions

An efficient new micromechanical model has been formulated by using a parametric finite-volume theory which is suitable for the evaluation of the effective thermal conductivity of periodic unidirectional composite materials with arbitrary internal architectural arrangements of fiber coated by thin interphase with low thermal conductivity. To demonstrate the performance of the model, examples of composite materials with different arrays, sizes and volume fractions of fibers have been presented. Size-dependence of the effective thermal conductivity of a composite with interfacial thermal resistance also has been investigated. Solutions obtained by the proposal model have been compared with analytical and finite element results. These comparisons show an excellent performance of the new model. Additionally, an investigation has been carried out on the range of interphase thermal conductivity for which the hypothesis of discontinuity in temperature and continuity in normal heat flux across the interfaces provides consistent solutions. Using as reference the results for the RUC constituted by three phases (matrix, fiber and interphase), it has been found that the mentioned hypothesis is capable of providing good results for interphase thermal conductivities beyond the range of low values in relation to the matrix thermal conductivity. In the most of the analyzed cases, that hypothesis provided satisfactory results for interphase thermal conductivity in the order of ten times the matrix thermal conductivity.

Acknowledgements

The authors acknowledge the financial support provided by the Brazilian federal agencies CNPq and CAPES.

References

1. Thornburg JD and Pears CD. *Prediction of the thermal conductivity of filled and reinforced plastics*. New York: ASME; 1965.
2. Springer GS and Tsai SW. Thermal conductivities of unidirectional materials. *Journal of Composite Materials.* 1967; 1(2):166-173. http://dx.doi.org/10.1177/002199836700100206.
3. Peng Y, Chiping J, Fan S and Xianghong X. Estimation of Transverse Thermal Conductivity of Doubly-Periodic Fiber

Reinforced Composites. *Chinese Journal of Aeronautics*. 2010; 23(1):54-60. http://dx.doi.org/10.1016/S1000-9361(09)60187-4.

4. Luciano R and Barbero EJ. Formulas for the stiffness of composites with periodic microstructure. *International Journal of Solids and Structures*. 1994; 31(21):2933-2944. http://dx.doi.org/10.1016/0020-7683(94)90060-4.
5. Rolfes R and Hammerschmidt U. Transverse thermal conductivity of CFRP laminates: a numerical and experimental validation of approximation formulae. *Composites Science and Technology*. 1995; 54(1):45-54. http://dx.doi.org/10.1016/0266-3538(95)00036-4.
6. Sihn S and Roy AK. Micromechanical analysis for transverse thermal conductivity of composites. *Journal of Composite Materials*. 2011; 45(11):1245-1255. http://dx.doi.org/10.1177/0021998310382311.
7. Cavalcante MAA, Marques SPC and Pindera M-J. Parametric Formulation of the Finite-Volume Theory for Functionally Graded Materials. Part I: Analysis. *ASME Journal of Applied Mechanics*. 2007; 74(5):935-945. http://dx.doi.org/10.1115/1.2722312.
8. Bansal Y and Pindera M-J. Efficient Reformulation of the Thermoelastic Higher - Order Theory for Functionally Graded Materials. *Journal of Thermal Stresses*. 2003; 26(11-12):1055-1092. http://dx.doi.org/10.1080/714050872.
9. Gattu M, Khatam H, Drago AS and Pindera M-J. Parametric Finite-Volume Micromechanics of Uniaxial Continuously-Reinforced Periodic Materials with Elastic Phases. *Journal of Engineering Materials and Technology*. 2008; 130(3). http://dx.doi.org/10.1115/1.2931157.
10. Khatam H and Pindera M-J. Parametric Finite-Volume Micromechanics of Periodic Materials with Elastoplastic Phases. *International Journal of Plasticity*. 2009; 25(7):1386-1411. http://dx.doi.org/10.1016/j.ijplas.2008.09.003.
11. Cavalcante MAA, Khatam H and Pindera M-J. Homogenization of elastic-plastic periodic materials by FVDAM and FE approaches - An assessment. *Composites. Part B, Engineering*. 2011; 42(6):1713-1730. http://dx.doi.org/10.1016/j.compositesb.2011.03.006.
12. Yvonnet J, He Q-C, Zhu Q-Z and Shao J-F. A general and efficient computational procedure for modeling the Kapitza thermal resistance based on XFEM. *Computational Materials Science*. 2011; 50(4):1220-1224. http://dx.doi.org/10.1016/j.commatsci.2010.02.040.
13. Hashin Z. Thin interphase/imperfect interface in conduction. *Journal of Applied Physics*. 2001; 89(4):2261-2267. http://dx.doi.org/10.1063/1.1337936.
14. Benveniste Y. A general interface model for a three-dimensional curved thin anisotropic interphase between two anisotropic media. *Journal of the Mechanics and Physics of Solids*. 2006; 54(4):708-734. http://dx.doi.org/10.1016/j.jmps.2005.10.009.
15. Nan CW, Birringer R, Clarke DR and Gleiter H. Effective thermal conductivity of particulate composites with interfacial thermal resistance. *Journal of Applied Physics*. 1997; 81(10):6692-6699. http://dx.doi.org/10.1063/1.365209.